Comput. Methods Appl. Mech. Engrg. 268 (2014) 126–140

Contents lists available at ScienceDirect

Comput. Methods Appl. Mech. Engrg.

journal homepage: www.elsevier.com/locate/cma

The discontinuous enrichment method for medium-frequency Helmholtz problems with a spatially variable wavenumber

Radek Tezaur [a,*], Irina Kalashnikova [b], Charbel Farhat [a]

[a] Department of Aeronautics and Astronautics, Stanford University, Stanford, CA 94305, USA
[b] Numerical Analysis and Applications Department, Sandia National Laboratories, Albuquerque, NM 87185, USA

ARTICLE INFO

Article history:
Received 25 January 2013
Received in revised form 15 August 2013
Accepted 19 August 2013
Available online 20 September 2013

Keywords:
Acoustics
Discontinuous enrichment method
Helmholtz
High-order methods
Medium frequency regime
Variable wavenumber

ABSTRACT

Numerical dispersion, or what is often referred to as the pollution effect, presents a challenge to an efficient finite element discretization of the Helmholtz equation in the medium frequency regime. To alleviate this effect and improve the unsatisfactory pre-asymptotic convergence of the classical Galerkin finite element method based on piecewise polynomial basis functions, several discretization methods based on plane wave bases have been proposed. Among them is the discontinuous enrichment method that has been shown to offer superior performance to the classical Galerkin finite element method for a number of constant wavenumber Helmholtz problems and has also outperformed two representative methods that use plane waves – the partition of unity and the ultra-weak variation formulation methods. In this paper, the discontinuous enrichment method is extended to the variable wavenumber Helmholtz equation. To this effect, the concept of enrichment functions based on free-space solutions of the homogeneous form of the governing differential equation is enlarged to include free-space solutions of approximations of this equation obtained in this case by successive Taylor series expansions of the wavenumber around a reference point. This leads to plane wave enrichment functions based on the piece-wise constant approximation of the wavenumber, and to Airy wave enrichment functions. Several elements based on these enrichment functions are constructed and evaluated on benchmark problems modeling sound-hard scattering by a disk submerged in an acoustic fluid where the speed of sound varies in space. All these elements are shown to outperform by a substantial margin their continuous polynomial counterparts.

1. Introduction

The Helmholtz equation models the time harmonic form of the wave equation. As such, its applications range from acoustics and electromagnetics, to aerodynamics and quantum mechanics. Traditional discretization methods such as the standard Galerkin finite element method (FEM) are well-suited for elliptic boundary value problems such as the Helmholtz equation, but their scalability with respect to the wavenumber κ is unsatisfactory. In particular, due to numerical dispersion, traditional methods have difficulties computing the numerical solution accurately and efficiently at medium and high frequencies. In this regime, the solution is highly oscillatory and features many wavelengths within the computational domain. More specifically, it has been shown that the error of a finite element approximation with linear elements scales as $O(\kappa(\kappa h)^2)$, where h denotes the element size [14]. It is thus insufficient to keep the same number of elements per wavelength (i.e., keep κh constant) as the wavenumber is increased. This phenomenon, known as the pollution effect, combined with the

* Corresponding author. Tel.: +1 6507259646.
E-mail address: rtezaur@stanford.edu (R. Tezaur).

0045-7825/$ - see front matter © 2013 Elsevier B.V. All rights reserved.
http://dx.doi.org/10.1016/j.cma.2013.08.017

fact that an increase in the frequency results in an increase in the number of wavelengths in the domain, makes the standard polynomial FEM unaffordable in the medium frequency regime.

Recent developments suggest that for a fixed computational cost, the performance of a numerical algorithm for the solution of the Helmholtz equation is greatly improved by taking advantage of *a priori* knowledge of the exact solution. For a problem with a constant wavenumber, instead of approximating a discrete solution using piece-wise polynomials, piecewise plane waves can be used, as these are known to be exact solutions of the homogeneous, free-space, Helmholtz equation with a spatially constant wavenumber. Examples of methods that use these plane wave basis functions include the ultra-weak variational formulation (UWVF) [2,13], the partition of unity method (PUM) [25,27,1,19,33], the discontinuous Galerkin method [10], the least squares method [26], the variational theory of complex rays [32,31,18], and the discontinuous enrichment method with Lagrange multipliers (DEM) [4]. (The concept of free space solutions is native to Trefftz methods, e.g. the wave based method [29] that uses a basis different from plane waves.) PUM is a continuous method that can be understood as a generalized version of the polynomial FEM where the basis functions consist of the product of plane waves and linear hat functions. The other methods are discontinuous – the basis functions are not constructed in a way that maintains continuity of the numerical solution across the element boundaries. Instead, the continuity across neighboring elements is maintained in a weak sense, by incorporating additional constraints into the variational formulation. For DEM, these constraints are enforced by Lagrange multipliers. In a direct comparison on a two-dimensional scattering problem, DEM has outperformed PUM and UWVF methods [37].

The discontinuous enrichment method was originally proposed in [4] for the solution of multi-scale boundary value problems (BVPs) with sharp gradients and oscillations. In this method, the standard finite element polynomial field, which can be seen as representing the coarse scale of the solution [5], is enriched within each element by free-space solutions of the homogeneous form of the partial differential equation (PDE) to be solved. Such enrichment functions can be interpreted as representing the fine scales of the solution. Because these functions are typically discontinuous across the element interfaces, Lagrange multipliers are introduced at the element interfaces to enforce a weak continuity of the solution. DEM has been benchmarked against the higher order polynomial FEM for the Helmholtz equation in both two dimensions (2D) [7] and three dimensions (3D) [35]. CPU speedup factors as large as 100 have been observed for a fixed accuracy in 3D. Although initially developed for quadrilateral and hexahedral elements, DEM can be applied on triangular meshes in 2D [11] and tetrahedral meshes in 3D [12] as well. The method has also been extended to other problems including interface problems with evanescent waves [36], structural vibrations [38,24], fluid–structure interaction [23], the wave equation [28], and advection–diffusion problems with constant [9] and non-constant [17,16] coefficients.

Even though a spatially constant wavenumber is encountered in many applications of the Helmholtz equation, others, for example, underwater acoustics in large domains and wave propagation in geophysics or electromagnetics, often feature a spatially variable wavenumber. Furthermore, whereas free-space solutions of the homogeneous Helmholtz equation with a constant wavenumber are easy to find analytically, this is not necessarily the case when the wavenumber varies in space. This raises the issue of how to generalize the aforementioned methods to the case of a variable wavenumber. Special solutions in the case of a layered material have been suggested in references [36,23] in the context of DEM, and in [22] in the context of UWVF; for treatment in the context of PUM, see references [20,21]. Here, the focus is set on the case of a smoothly variable wavenumber. Some progress has been reported for this case in one dimension (1D) [15] for the UWVF method: essentially, exponentials of polynomials have been explored to approximate the solution of the problem. In this paper, the issue raised by the lack of analytical free-space solutions of the homogeneous Helmholtz equation with a variable wavenumber is addressed by focusing on DEM and using free-space solutions of approximations of this governing equation of various orders. To this effect, the remainder of this paper is organized as follows.

Section 2 overviews the formulation of the discontinuous enrichment method and its discretization and computational aspects. Section 3 enlarges the concept of free-space solutions of the homogeneous form of a governing differential equation with a varying parameter as outlined above. This idea recovers as a particular case the piecewise constant approximation of the varying parameter that was previously suggested in [4,5] and explored in more detail in [17,16] for advection–diffusion problems. More importantly, the idea developed in this paper also leads to the Airy wave enrichment functions which are free-space solutions of the homogeneous Helmholtz equation when the square of the wavenumber is linearized around a reference point. Section 4 assesses the performance, for two model problems in the medium frequency regime, of various DEM elements constructed using the enrichment functions considered or proposed in this paper for the Helmholtz equation with a variable wave number. Finally, conclusions are drawn in Section 5.

2. Discontinuous enrichment method

2.1. Boundary value problem

The Helmholtz equation can be derived from the wave equation $\Delta U - \frac{1}{c^2}\partial_{tt}U = 0$, where t denotes time by assuming that the solution $U(\mathbf{x}, t)$ is time-harmonic with the angular frequency ω, i.e., $U(\mathbf{x}, t) = u(\mathbf{x})e^{-i\omega t}$, where $\mathbf{x}$ denotes the spatial coordinates. In acoustics, U represents small pressure oscillations around an equilibrium value, and c is the speed of sound. By denoting the wavenumber $\kappa = \omega/c$, the usual form of the Helmholtz equation, $-\Delta u - \kappa^2 u = 0$, where u is the unknown complex amplitude, is obtained.

The following Helmholtz BVP is considered here

$$\begin{aligned} -\Delta u - \kappa^2 u &= 0 \quad \text{in} \quad \Omega, \\ \frac{\partial u}{\partial \boldsymbol{\nu}} &= g_N \quad \text{on} \quad \partial\Omega_N, \\ \frac{\partial u}{\partial \boldsymbol{\nu}} - i\kappa u &= g_R \quad \text{on} \quad \partial\Omega_R, \end{aligned} \tag{1}$$

where $\boldsymbol{\nu}$ denotes the normal derivative on the domain boundary $\partial\Omega = \partial\Omega_N \cup \partial\Omega_R$, $\partial\Omega_N \cap \partial\Omega_R = \emptyset$, i is the imaginary unit, $i^2 = -1$, and g_N and g_R are prescribed Neumann and Robin data, respectively. The Robin boundary condition makes the problem well-posed for any positive value of the wavenumber κ [14]. It is often used as a simple approximation of the Sommerfeld boundary condition when an infinite medium is considered and the problem domain is truncated to facilitate treatment by finite elements. More accurate absorbing boundary conditions are available (for example, see [14,3,34]), and several of these have been successfully used in the context of DEM [8]. The Robin and Neumann boundary conditions given in the BVP (1) are used in the acoustic problems chosen in Section 4 for assessing the performance of the solution methods considered in this paper. However, incorporating a Dirichlet boundary condition in the formulation of DEM overviewed below is straightforward and has been discussed in the literature [9,17]. Also, attention is restricted in this work to two dimensions for the sake of simplicity, but without any loss of generality.

2.2. Hybrid variational formulation

Like any finite element method, the discontinuous enrichment method relies on a partitioning of the domain Ω into n_{el} subdomains (elements) such that $\overline{\Omega} = \cup_{j=1}^{n_{el}} \overline{\Omega}_j$ and $\Omega_j \cap \Omega_k = \emptyset$, $k \neq j$. Let $\Gamma_j = \partial\Omega_j$ be the boundary of Ω_j and let the edges between elements be denoted by $\Gamma_{jk} = \Gamma_j \cap \Gamma_k$, $j, k = 1, \ldots, n_{el}$. The formulation of DEM requires the introduction of two functional spaces: the space of functions representing the solution, denoted here by $\mathcal{U}$, and the space of approximation functions for the dual unknowns, the Lagrange multipliers, denoted here by $\mathcal{W}$. The functional space for the solution is allowed to have discontinuities across element edges, i.e.,

$$\mathcal{U} = \left\{ v \in L^2(\cup_{j=1}^{n_{el}} \Omega_j) : v|_{\Omega_j} \in H^1(\Omega_j) \right\}. \tag{2}$$

The space $\mathcal{W}$ of Lagrange multipliers, which are introduced on the edges between elements to enforce weakly the continuity of the solution, is defined as

$$\mathcal{W} = \prod_{k=1}^{n_{el}} \prod_{j=1 j<k}^{n_{el}} H^{-1/2}(\Gamma_{jk}). \tag{3}$$

With this notation in place, the hybrid variational formulation of DEM can be written as [4]: Find $(u, \lambda) \in \mathcal{U} \times \mathcal{W}$ such that

$$\begin{aligned} a(u, v) + b(\lambda, v) &= r(v) \quad \forall v \in \mathcal{U}, \\ b(\mu, u) &= 0 \quad \forall \mu \in \mathcal{W}, \end{aligned} \tag{4}$$

where a and b are two bilinear forms and r is a linear form. These are defined by

$$a(u, v) = \int_\Omega (\nabla u \cdot \nabla v - \kappa^2 u v)\, d\Omega - \int_{\partial\Omega_R} i\kappa u v\, d\Gamma, \tag{5}$$

$$b(\mu, v) = \sum_{k=1}^{n_{el}} \sum_{\substack{j=1 \\ j<k}}^{n_{el}} \int_{\Gamma_{jk}} \mu(v|_{\Omega_j} - v|_{\Omega_k})\, d\Gamma, \quad \text{and} \tag{6}$$

$$r(v) = \int_{\partial\Omega_N} v g_N\, d\Gamma + \int_{\partial\Omega_R} v g_R\, d\Gamma. \tag{7}$$

2.3. DEM discretization

In the discretization process, $\mathcal{U}$ and $\mathcal{W}$ are replaced by finite dimensional subspaces, $\mathcal{U}^h$ and $\mathcal{W}^h$, where h denotes the typical element size, and the resulting linear system of equations is solved for the degrees of freedom of the approximate solution. Choices of the approximation spaces are the subject of the next section. Here, general guidelines and practical considerations are discussed.

In [5], DEM is presented as a multiscale computational framework in which $\mathcal{U}^h = \mathcal{U}^E + \mathcal{U}^P$. The space $\mathcal{U}^P$ is a standard finite element polynomial space. Functions in $\mathcal{U}^P$ are continuous between elements and polynomial within each element; they are intended to capture the coarse scales of the solution. The enrichment space $\mathcal{U}^E$ is a space of discontinuous functions that are designed to capture oscillatory and/or high-gradient components of the solution that are computationally expensive to approximate using polynomials. Free-space solutions of the homogeneous PDE are suggested as good candidates for this space. For a

range of applications – primarily source-free problems such as scattering problems whose exact solution is not known to contain polynomials explicitly – it has been shown that the continuous polynomial field can be dropped from the approximation [7,8].

Denoting by $\mathbf{u}$ and $\boldsymbol{\lambda}$ the vectors of degrees of freedom of the approximate solution $u^h \in \mathcal{U}^h$ and the approximate Lagrange multiplier $\lambda^h \in \mathcal{W}^h$, respectively, the hybrid variational formulation leads to the linear system of equations

$$\begin{bmatrix} \mathbf{K} & \mathbf{C} \\ \mathbf{C}^T & \mathbf{0} \end{bmatrix} \begin{bmatrix} \mathbf{u} \\ \boldsymbol{\lambda} \end{bmatrix} = \begin{bmatrix} \mathbf{r} \\ \mathbf{0} \end{bmatrix}, \tag{8}$$

where the matrix $\mathbf{K}$ is associated with $a(u^h, v^h)$, the matrix $\mathbf{C}$ with $b(\lambda^h, v^h)$, and the right hand side vector $\mathbf{r}$ with $r(v^h)$.

When the basis functions used to approximate the solution are not continuous across neighboring elements, the corresponding degrees of freedom associated with one element are decoupled from those of another element. Thus, these degrees of freedom can be condensed out at the element level. Assuming for notational simplicity that this is the case for all degrees of freedom corresponding to functions in $\mathcal{U}^h$ – in other words, assuming that $\mathcal{U}^P = \emptyset$ or that the polynomial functions of $\mathcal{U}^P$ are also discontinuous – the local matrices after static condensation are assembled into the following global dual system which governs the Lagrange multiplier degrees of freedom only

$$\mathbf{C}^T\mathbf{K}^{-1}\mathbf{C}\boldsymbol{\lambda} = \mathbf{C}^T\mathbf{K}^{-1}\mathbf{r}. \tag{9}$$

The primal solution vector is then obtained by computing in post-processing mode

$$\mathbf{u} = \mathbf{K}^{-1}(\mathbf{r} - \mathbf{C}\boldsymbol{\lambda})$$

at the element level ($\mathbf{K}$ is in this case a block diagonal matrix). Since the cost of local assembly and local static condensation scales linearly with the number of elements, the computational cost of the method is, for large problems, determined mostly by the cost of solving the system (9) for the Lagrange multiplier degrees of freedom. This cost estimate is particularly accurate on parallel computing platforms because the local element operations are massively parallelizable.

By applying integration by parts to the definition of $a(u, v)$ and substituting the result into the first of Eq. (4), one obtains $\lambda = \frac{\partial u}{\partial \nu}$. This suggests that λ should be discretized as a good approximation of the normal derivative of the solution which is in the discrete case approximated by a linear combination of the enrichment functions [6,8]. However, assigning as many Lagrange multiplier degrees of freedom per element edge as there are enrichment degrees of freedom within that element is not only computationally inefficient, but also leads to a singular global system. Farhat et al. [6] have shown that, for a square mesh, a necessary algebraic condition is $n_\lambda \leqslant \frac{n_w}{2}$, where n_λ is a number of Lagrange multiplier degrees of freedom on each element edge and n_w is a number enrichment functions per element. This condition partially addresses the *inf-sup* condition by maintaining the total number of constraints (Lagrange multipliers) smaller than the total number of enrichment variables.

3. Choice of approximation spaces for variable wavenumber problems

Plane waves of the form $e^{i\kappa \mathbf{d}\cdot\mathbf{x}}$, where $\mathbf{d}$ is a unitary vector defining a direction of propagation, are free-space solutions of the homogeneous Helmholtz equation with a constant wavenumber. DEM constructs the enrichment space for a Helmholtz problem characterized by a constant wavenumber as a set of waves propagating in different directions that are chosen *a priori*. When the wavenumber varies in space, the plane waves identified above are no longer free-space solutions of the homogeneous Helmholtz equation. Furthermore, free-space solutions to the variable wavenumber Helmholtz equation are hard to find in general. For this reason, the concept of free-space solutions of the homogeneous form of the governing equation is expanded here to include approximations of such solutions. In particular, free-space solutions of approximations of various orders of accuracy of the homogeneous form of the governing equation are considered. For the case of a Helmholtz problem with a spatially variable wavenumber $\kappa(\mathbf{x}) \in C^2(\Omega_j)$, two approximations of the homogeneous form of the governing equation, for which free-space solutions can be derived analytically, are obtained by approximating within each element Ω_j the square of the wavenumber, $\kappa^2(\mathbf{x})$, by its Taylor series expansions of order 0 and 1 around a reference point $\mathbf{x}_j$ in Ω_j (practically, the midpoint is chosen). Indeed, the expansions

$$\kappa^2(\mathbf{x}) = \kappa^2(\mathbf{x}_j) + \zeta\nabla(\kappa^2)|_{\mathbf{x}=\mathbf{x}_j} \cdot (\mathbf{x} - \mathbf{x}_j) + \mathcal{O}\left(\|\mathbf{x} - \mathbf{x}_j\|^{(1+\zeta)}\right) \quad \text{in } \Omega_j, \tag{10}$$

where $\nabla\kappa^2|_{\mathbf{x}=\mathbf{x}_j} \equiv \left(\frac{\partial\kappa^2}{\partial x}(\mathbf{x}_j), \frac{\partial\kappa^2}{\partial y}(\mathbf{x}_j)\right)^T$ and the superscript T denotes the transpose operation, lead to

$$-\Delta u - \left(\kappa^2(\mathbf{x}_j) + \zeta\nabla(\kappa^2)|_{\mathbf{x}=\mathbf{x}_j} \cdot (\mathbf{x} - \mathbf{x}_j)\right)u = \mathcal{O}\left(\|\mathbf{x} - \mathbf{x}_j\|^{(1+\zeta)}\right)u, \tag{11}$$

where $\zeta = 0$ or 1 for the Taylor series of order 0 or 1. The free-space solutions of the homogeneous form of Eq. (11) and the choice of approximation spaces they lead to for the discretization by DEM are pursued in Sections 3.1 and 3.2 for $\zeta = 0$ and $\zeta = 1$, respectively.

Unlike the governing equation of the BVP (1), the alternative Eq. (11) has a non-zero source term. In [5], it was suggested that for a right hand side that induces a slowly varying component of the solution (coarse scale), the polynomial component in the DEM approximation be kept as it can represent this coarse scale component more efficiently than oscillatory functions

that form the fine scale. However, the source term in Eq. (11) is proportional to the sought-after solution u and therefore does not introduce in this solution a coarser scale. Hence, keeping or dropping in this case the polynomial component of the DEM approximation must be decided based on other considerations. Here, the following reasoning is adopted for this purpose:

- For $\zeta = 0$, the low-order approximation of the homogeneous form of the governing Helmholtz Eq. (11) is not necessarily expected to be adequate and therefore its corresponding free-space solutions are not expected to be as efficient as the enrichment functions obtained for a Helmholtz problem with a constant wavenumber. Thus, the polynomial component is maintained in the approximation. However, it is chosen here to be discontinuous for two reasons: (1) it is considered in this case to remedy element-by-element the imperfections of the free-space solutions of the approximate equation as these vary from element to element; (2) this enables the elimination of the polynomial component at the element level and therefore yields a smaller and sparser global system of equations. In order to highlight the importance of the polynomial component of the DEM approximation when $\zeta = 0$, elements without the polynomial field are also considered in the numerical examples of Section 4.
- For $\zeta = 1$, it is anticipated that the higher-order approximation of the homogeneous form of the governing Helmholtz equation will be more effective than its first-order counterpart. Therefore, the polynomial component is omitted because in this case the source term $\mathcal{O}\left(\|\mathbf{x} - \mathbf{x}_j\|^2\right)u$ has a very small magnitude (much smaller than for $\zeta = 0$) and therefore is not expected to significantly contribute to the solution of the BVP (1).

Throughout the remainder of this paper, a quadrilateral DEM element with n_w functions per element for the approximation of the primal variable and n_λ discrete Lagrange multipliers per edge is denoted by Q^ζ-n_w-n_λ, where "Q" stands for quadrilateral and the integer superscript ζ characterizes the method used to design the spaces of approximation of this element. A similar quadrilateral element which features however an additional polynomial field is denoted by Q^ζ-n_w-p-n_λ, where p denotes the degree of the polynomial field. Similarly, a standard finite element based on a tensor product of polynomial approximation of degree p is denoted in the remainder of this paper by Q_p. For example, the elements Q^ζ-8-2 and Q^ζ-16-4 are graphically depicted in Fig. 1.

3.1. Approximation spaces based on the piece-wise constant approximation of the wavenumber

For $\zeta = 0$, the wavenumber in Eq. (11) becomes constant within an element Ω_j and the plane waves with $\kappa \equiv \kappa(\mathbf{x}_j)$ solve the corresponding homogeneous equation. Hence in this case, the DEM approximation space $\mathcal{U}^h$ is constructed as

$$\mathcal{U}^h = \mathcal{U}^e \oplus \widehat{\mathrm{Q}}_p \tag{12}$$

where $\widehat{\mathrm{Q}}_p$ is the discontinuous equivalent of the tensor-product polynomial space Q_p,

$$\mathcal{U}^e = \left\{ u^h \in L^2(\Omega) : u^h(\mathbf{x})|_{\Omega_j} = \sum_{q=1}^{n_{w,j}} e^{i\kappa(\mathbf{x}_j)\mathbf{d}_{jq}\cdot\mathbf{x}} u_{jq}, \mathbf{x}_j \in \Omega_j, u_{jq} \in \mathbb{C}, j = 1, \ldots, n_{el} \right\}, \tag{13}$$

and $n_{w,j}$ denotes the number of plane wave functions in the element Ω_j. In the absence of some *a priori* knowledge of the solution, $n_{w,j}$ is chosen to have the same value n_w in all elements of the mesh, the angles ϕ_{jq} are typically chosen to be uniformly distributed and the same in all elements – i.e., $\phi_{jq} = (q-1)2\pi/n_w,\ q = 1, \ldots, n_w,\ j = 1, \ldots, n_{el}$.

The space (13) described above follows the idea suggested in the founding papers of DEM [4,5] for constructing an enrichment basis when the governing equation has variable coefficients and the homogeneous form of its constant coefficient counterpart has analytical free-space solutions. This idea consists in freezing within each element the variable coefficients so that the aforementioned free-space solutions can be used to construct a basis of enrichment functions. Furthermore, the choice (13) is the same as that adopted in [7,8] for constructing DEM elements for the solution of the Helmholtz equation with a constant wavenumber. Hence, the approximation space for the Lagrange multipliers is chosen here to be virtually

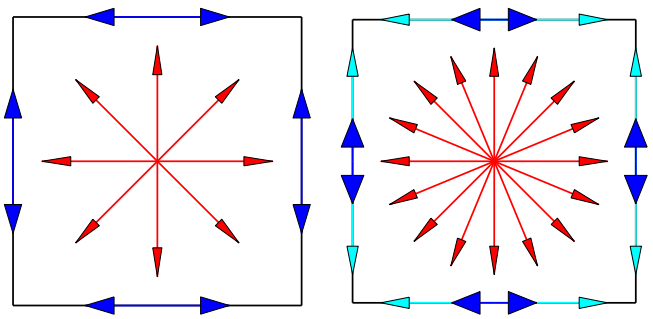

Fig. 1. The quadrilateral elements Q^ζ-8-2 (left) and Q^ζ-16-4 (right).

the same as that developed in [7,8], with the exception that the wavenumber is allowed in this case to vary along an element edge. This leads to

$$\mathcal{W}^h = \left\{ \lambda^h \in \mathcal{W} : \lambda^h(\mathbf{x}(s))|_{\Gamma_{jk}} = \sum_{q=1}^{n_\lambda} e^{i\kappa(\mathbf{x}(s))c_q s} \lambda_{jk,q}, \mathbf{x}(s) \in \Gamma_{jk}, \lambda_{kj,q} \in \mathbb{C}, j,k = 1,\ldots,n_{el} \right\}, \tag{14}$$

where s is the curvilinear abscissa along an edge and c_q are coefficients, determined by an optimization procedure (see [7,8]) and given below.

Using the templates of the approximation spaces (12) and (14) with specific combinations of n_w and n_λ, the DEM elements Q^0-4-p-1, Q^0-8-p-2, Q^0-12-p-3, Q^0-16-p-4, and Q^0-20-p-5 are constructed for the solution of the Helmholtz equation with a spatially variable wavenumber. Here, the superscript 0 refers to $\zeta = 0$. The counterparts of these elements that do not include the discontinuous polynomial contribution $\widehat{Q}_p$, i.e. where $\mathcal{U}^h = \mathcal{U}^e$, are the elements Q^0-4-1, Q^0-8-2, Q^0-12-3, Q^0-16-4, and Q^0-20-5. As stated earlier, these elements are considered here only for the purpose of highlighting the importance of the polynomial contribution. For a constant wavenumber, the approximation spaces given in (13) and (14) simplify to those proposed in [7,8]. Consistently with this observation, the DEM elements Q^0-4-1, Q^0-8-2, and Q^0-16-4 simplify in this case, respectively, to the elements Q-4-1, Q-8-2, and Q-16-4 introduced in [6–8]. The DEM element Q^0-12-3 becomes identical to the element Q-12-3 introduced in [37], and the element Q^0-20-5 is added here for the first time. It is also noted that for the case of a constant wave number, all aforementioned DEM elements were shown to possess good approximation and stability properties. Here, their generalization to the case of spatially variable wavenumbers is equipped with the following values of the coefficients c_q introduced in (14).

- Q^0-4-p-1 and Q^0-4-1: $c_1 = 0$.
- Q^0-8-p-2 and Q^0-8-2: $c_1 = -0.5,\ c_2 = 0.5$.
- Q^0-12-p-3 and Q^0-12-3: $c_1 = -0.707,\ c_2 = 0,\ c_3 = 0.707$.
- Q^0-16-p-4 and Q^0-16-4: $c_1 = -0.75,\ c_2 = -0.2,\ c_3 = 0.2, c_4 = 0.75$.
- Q^0-20-p-5 and Q^0-20-5: $c_1 = -0.9,\ c_2 = -0.5,\ c_3 = 0.0,\ c_4 = 0.5,\ c_5 = 0.9$.

3.2. Approximation spaces based on the piece-wise linear approximation of the wavenumber: the Airy functions

For $\zeta = 1$, the wavenumber varies linearly within the element. Motivated by the plane waves used in the constant wavenumber case, a basis of solutions resembling plane waves propagating in uniformly distributed directions is sought. To derive such a function for a particular direction, a local coordinate system aligned with the direction is considered and free-space solutions of the homogeneous form of Eq. (11) are obtained analytically using the method of separation of variables. More basis functions can then be created by considering different angles of rotation. To this effect, consider the coordinate system $(\tilde{x}, \tilde{y})$ centered at the linearization point $\mathbf{x}_j = (x_j, y_j)$ and rotated by an angle ϕ with respect to the global coordinate system – that is,

$$\begin{bmatrix} \tilde{x} \\ \tilde{y} \end{bmatrix} = \begin{bmatrix} \cos\phi & -\sin\phi \\ \sin\phi & \cos\phi \end{bmatrix} \begin{bmatrix} x - x_j \\ y - y_j \end{bmatrix}.$$

In this rotated coordinate system, the linearized Helmholtz equation can be rewritten as

$$\Delta u + (\alpha\tilde{x} + \beta\tilde{y} + \gamma)u = 0, \tag{15}$$

where

$$\alpha = \frac{\partial\kappa^2}{\partial\tilde{x}}(0,0), \quad \beta = \frac{\partial\kappa^2}{\partial\tilde{y}}(0,0), \quad \text{and} \quad \gamma = \kappa^2(0,0).$$

Searching for a solution of this equation of the form

$$u(\tilde{x},\tilde{y}) = F(\tilde{x})G(\tilde{y}) \tag{16}$$

leads to

$$\left(\frac{F''}{F} + \alpha\tilde{x} + \gamma\right) = -\left(\frac{G''}{G} + \beta\tilde{y}\right) \equiv \delta, \tag{17}$$

where F'' and G'' denote the second derivatives of F and G with respect to their variables, respectively, and $\delta \in \mathbb{R}$ is a free parameter. Eq. (17) give rise to the ordinary differential equations

$$F'' + (\alpha\tilde{x} + \gamma - \delta)F = 0 \quad \text{and} \tag{18}$$

$$G'' + (\beta\tilde{y} + \delta)G = 0, \tag{19}$$

which are two variants of the Airy equation [30]. The reader can verify that the following functions are solutions of the above equations

$$F(\tilde{x}) = \begin{cases} C_1 \mathrm{Ai}\left(\frac{-\alpha\tilde{x}-\gamma+\delta}{\alpha^{2/3}}\right) + C_2 \mathrm{Bi}\left(\frac{-\alpha\tilde{x}-\gamma+\delta}{\alpha^{2/3}}\right) & \alpha \neq 0 \\ C_1 \cos\left(\sqrt{\gamma-\delta}\tilde{x}\right) + C_2 \sin\left(\sqrt{\gamma-\delta}\tilde{x}\right) & \alpha = 0 \end{cases} \tag{20}$$

and

$$G(\tilde{y}) = \begin{cases} D_1 \mathrm{Ai}\left(\frac{-\beta\tilde{y}-\delta}{\beta^{2/3}}\right) + D_2 \mathrm{Bi}\left(\frac{-\beta\tilde{y}-\delta}{\beta^{2/3}}\right) & \beta \neq 0 \\ D_1 \cos\left(\sqrt{\delta}\tilde{y}\right) + D_2 \sin\left(\sqrt{\delta}\tilde{y}\right) & \beta = 0 \end{cases}, \tag{21}$$

where $\mathrm{Ai}(\cdot)$ and $\mathrm{Bi}(\cdot)$ denote the so-called Airy functions and $C_1,\ C_2,\ D_1,\ D_2$ are arbitrary constants.

The Airy functions Ai and Bi are displayed in Fig. 2. They are oscillatory on the negative axis. For $x \to -\infty$, they can be related to scaled sine and cosine functions.

There is a lot of freedom in selecting the constants in Eqs. (20) and (21). In the context of this work, free-space solutions of the homogeneous form of Eq. (11) with $\zeta = 1$ in a form close to that of a plane wave are sought. In the rotated coordinate system, such a solution is oscillatory along $\tilde{x}$ rather than decaying, and varies only slowly in the $\tilde{y}$ direction. These considerations lead to choosing $\delta = 0,\ G(0) = 1$, and $G'(0) = 0$, which determines uniquely the constants D_1 and D_2. Then, two functions $u(\tilde{x}, \tilde{y})$ are obtained from (16) by choosing $(C_1 = 1, C_2 = 0)$ and $(C_1 = 0, C_2 = 1)$ in (20). These are denoted here by $\mathrm{Ai}(\mathbf{x}_j, \phi; \mathbf{x})$ and $\mathrm{Bi}(\mathbf{x}_j, \phi; \mathbf{x})$, respectively, and referred to as Airy (plane) waves. Their parameters $\mathbf{x}_j$ and ϕ underline their dependence on the linearization point and the rotation of the coordinate system. Both functions are displayed in Fig. 3 for $\kappa^2(0,0) = 20$ and $\nabla\kappa^2(0,0) = (4,0)$, and for $\phi = 0$ (top) and $\phi = \pi/2$ (bottom). For $\phi = 0$, both Airy plane waves behave like a plane wave propagating in the x direction with a variable wavenumber. For $\phi = \pi/2$, both Airy plane waves propagate in the y direction but also exhibit some variation in the x direction.

Using the Airy plane waves derived above, the enrichment space of DEM (discrete subspace of (2)) is constructed as follows

$$\mathcal{U}^h = \left\{ u^h \in L^2(\Omega) : u^h(\mathbf{x})|_{\Omega_j} = \sum_{q=1}^{n_{wj}/2} \mathrm{Ai}(\mathbf{x}_j, \phi_{jq}; \mathbf{x}) u_{jq} + \mathrm{Bi}(\mathbf{x}_j, \phi_{jq}; \mathbf{x}) v_{jq}, \mathbf{x}_j \in \Omega_j, u_{jq}, v_{jq} \in \mathbb{C}, j = 1, \ldots, n_{el} \right\}. \tag{22}$$

Again, in the absence of some *a priori* knowledge of the solution, the parameters n_{wj} are set to $n_{wj} = n_w$, the number of enrichment functions per element n_w is chosen to be an even number, and the angles ϕ_{jq} are chosen to be the same in all elements and uniformly distributed between 0 and π – i.e., $\phi_{jq} = (q-1)\pi/(n_w/2),\ q = 1, \ldots, n_w/2,\ j = 1, \ldots, n_{el}$.

For $\alpha = 0$ in (20), F becomes a linear combination of sine and cosine functions that spans the same subspace as two plane waves. More specifically, $\cos\left(\sqrt{\gamma}\tilde{x}\right)$ and $\sin\left(\sqrt{\gamma}\tilde{x}\right)$ span the same subspace as $e^{i\sqrt{\gamma}\tilde{x}} = e^{i\sqrt{\gamma}\mathbf{x}\cdot(\cos\phi, \sin\phi)}$ and $e^{-i\sqrt{\gamma}\tilde{x}} = e^{i\sqrt{\gamma}\mathbf{x}\cdot(\cos(\pi+\phi), \sin(\pi+\phi))}$, respectively. If $\beta = 0$, then $G = 1$ and the Airy basis functions become independent of $\tilde{y}$. Thus, for $\alpha = \beta = 0$, the proposed basis is equivalent to the basis of plane waves.

Like the space of enrichment functions, the space of Lagrange multipliers is modeled here after its counterpart constructed for the case of a constant wavenumber. In the latter case, each Lagrange multiplier basis function can be interpreted as the normal derivative of a plane wave propagating at an angle ψ with the interface between two elements (for example, see (14) with a constant wavenumber $\kappa(\mathbf{x}(s)) = \kappa$) – that is, a function of the form found in the enrichment space. Two plane waves propagating at the angles $\pm\psi$ give rise to the same Lagrange multiplier function on the interface. This property is desirable because it makes the construction of the Lagrange multiplier basis functions independent of the order in which two elements sharing an edge are processed.

It turns out that for the case of a variable wavenumber, constructing the Lagrange multiplier basis functions directly from $\mathrm{Ai}(\cdot, \cdot; \mathbf{x})$ and $\mathrm{Bi}(\cdot, \cdot; \mathbf{x})$ does not provide the desired invariance property described above. Indeed, if θ_{jk} denotes the angle

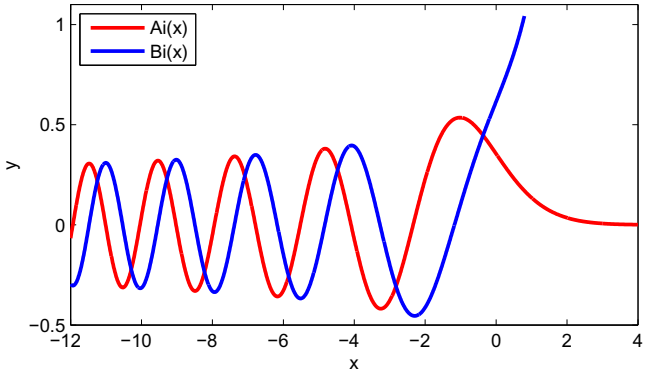

Fig. 2. Airy functions Ai and Bi.

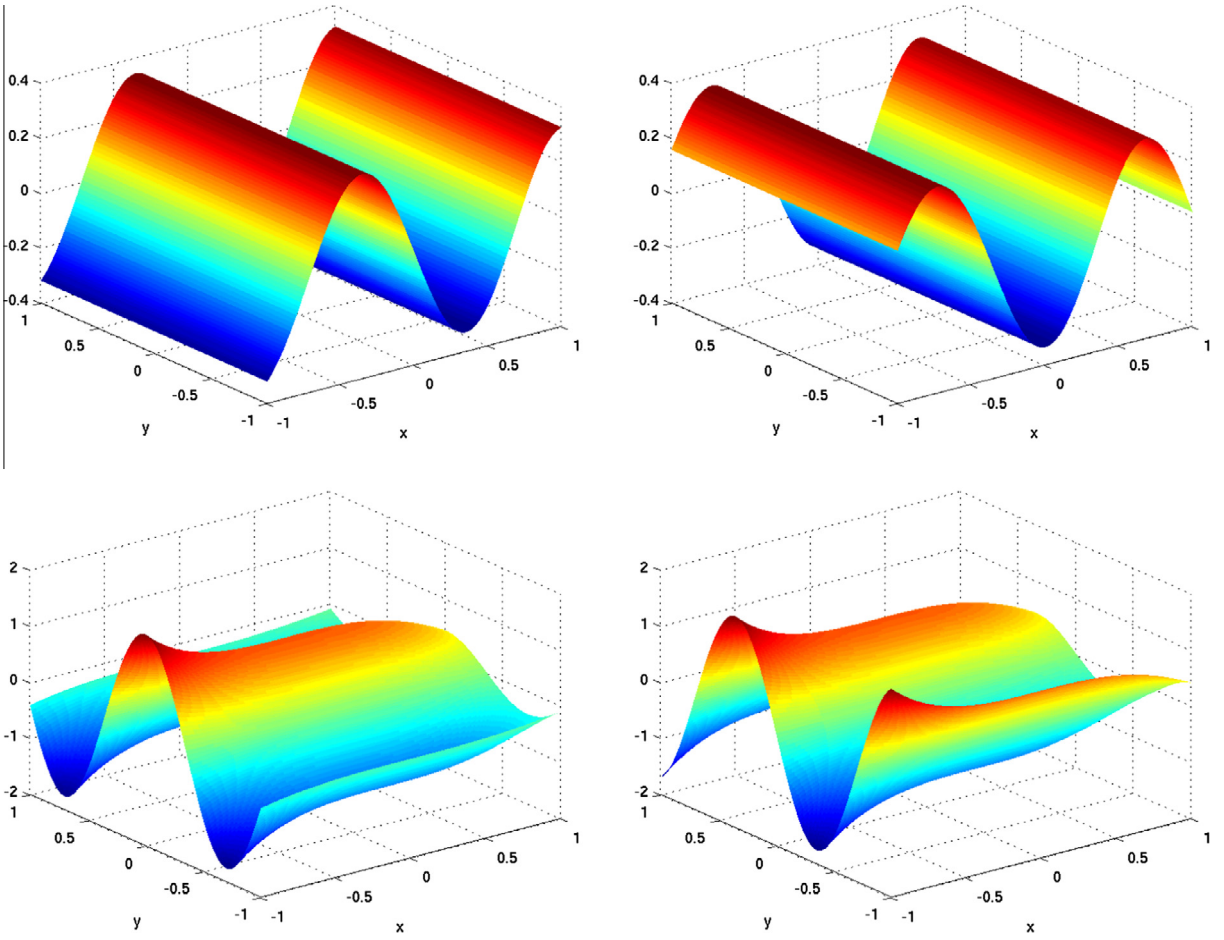

Fig. 3. Airy plane waves: left to right and top to bottom, $\mathrm{Ai}((0,0),0;\mathbf{x})$, $\mathrm{Bi}((0,0),0;\mathbf{x})$, $\mathrm{Ai}((0,0),\pi/2;\mathbf{x})$, $\mathrm{Bi}((0,0),\pi/2;\mathbf{x})$ for $\kappa^2(0,0)=20$ and $\nabla\kappa^2(0,0)=(4,0)$.

between the interface Γ_{jk} and the x-axis, and $\mathbf{x}_{jk}$ is a reference point for the linearization of the wavenumber κ introduced on this interface for the sake of constructing the Lagrange multiplier basis functions, then

$$\frac{\partial \mathrm{Ai}(\mathbf{x}_{jk},\theta_{jk}+\psi;\cdot)}{\partial \boldsymbol{\nu}} \neq \frac{\partial \mathrm{Ai}(\mathbf{x}_{jk},\theta_{jk}-\psi;\cdot)}{\partial \boldsymbol{\nu}}, \quad \text{and} \quad \frac{\partial \mathrm{Bi}(\mathbf{x}_{jk},\theta_{jk}+\psi;\cdot)}{\partial \boldsymbol{\nu}} \neq \frac{\partial \mathrm{Bi}(\mathbf{x}_{jk},\theta_{jk}-\psi;\cdot)}{\partial \boldsymbol{\nu}}.$$

This issue can be addressed by adopting an arithmetic average of the normal derivatives of the Airy plane waves. Because of the construction process of these waves described above, this issue can also be addressed by working with an arithmetic average of these waves themselves. However, it turns out that averaging directly the Airy plane waves associated with the angles $\mp\psi$ is not necessarily a good idea because occasionally, these waves can be in opposite phases. Therefore, the approach chosen here for addressing the invariance issue highlighted above begins with addressing the opposite phase problem by combining first the functions A_i and B_i as follows

$$\begin{aligned}\mathrm{Ci}(\mathbf{x}_{jk},\theta_{jk}\pm\psi;\cdot) &\equiv c_A^{\pm}\mathrm{Ai}(\mathbf{x}_{jk},\theta_{jk}\pm\psi;\cdot)+c_B^{\pm}\mathrm{Bi}(\mathbf{x}_{jk},\theta_{jk}\pm\psi;\cdot)\\ &\text{and}\\ \mathrm{Si}(\mathbf{x}_{jk},\theta_{jk}\pm\psi;\cdot) &\equiv d_A^{\pm}\mathrm{Ai}(\mathbf{x}_{jk},\theta_{jk}\pm\psi;\cdot)+d_B^{\pm}\mathrm{Bi}(\mathbf{x}_{jk},\theta_{jk}\pm\psi;\cdot).\end{aligned}$$

Then, the constant coefficients c_A^+, c_A^-, c_B^+, c_B^-, d_A^+, d_A^-, d_B^+, and d_B^- are chosen so that the resulting functions $\mathrm{Ci}(\mathbf{x}_{jk},\theta_{jk}\pm\psi;\cdot)$ and $\mathrm{Si}(\mathbf{x}_{jk},\theta_{jk}\pm\psi;\cdot)$ resemble the sine and cosine functions, respectively, near the point $\mathbf{x}_{jk}$ along the lines at the angles $\pm\psi$ with the interface Γ_{jk}, i.e.,

$$\mathrm{Ci}(\mathbf{x}_{jk},\theta_{jk}\pm\psi;\mathbf{x}_{jk})=1, \quad \text{and} \quad \mathrm{Ci}_{,\theta_{jk}\pm\psi}(\mathbf{x}_{jk},\theta_{jk}\pm\psi;\mathbf{x}_{jk})=0,$$

and

$$\mathrm{Si}(\mathbf{x}_{jk}, \theta_{jk} \pm \psi; \mathbf{x}_{jk}) = 0, \quad \text{and} \quad \mathrm{Si}_{,\theta_{jk}\pm\psi}(\mathbf{x}_{jk}, \theta_{jk} \pm \psi; \mathbf{x}_{jk}) = 1.$$

In the above equations, $f_{,\theta_{jk}\pm\psi}$ denotes the derivative of f in the direction of the vector $(\cos(\theta_{jk} \pm \psi), \sin(\theta_{jk} \pm \psi))$. Finally, two Lagrange multiplier basis functions corresponding to each sampled value of the angle ψ are formed – one as the average of the normal derivatives of the functions $\mathrm{Ci}(\mathbf{x}_{jk}, \theta_{jk} \pm \psi; \cdot)$ and the other as an average of the normal derivatives of the functions $\mathrm{Si}(\mathbf{x}_{jk}, \theta_{jk} \pm \psi; \cdot)$.

In summary for $\zeta = 1$, the proposed space of enrichment functions of DEM is that given in (22), and the proposed corresponding space of approximation of the Lagrange multiplier field is

$$\mathcal{W}_a^h = \left\{ \lambda^h \in \mathcal{W} : \lambda^h(\mathbf{x})|_{\Gamma_{jk}} = \sum_{q=1}^{\lceil n_\lambda/2 \rceil} \left(\frac{\partial \mathrm{Ci}(\mathbf{x}_{jk}, \theta_{jk} + \psi_q; \mathbf{x})}{\partial \boldsymbol{\nu}} + \frac{\partial \mathrm{Ci}(\mathbf{x}_{jk}, \theta_{jk} - \psi_q; \mathbf{x})}{\partial \boldsymbol{\nu}} \right) \lambda_{jk,q} \right.$$
$$\left. + \sum_{q=1}^{\lfloor n_\lambda/2 \rfloor} \left(\frac{\partial \mathrm{Si}(\mathbf{x}_{jk}, \theta_{jk} + \psi_q; \mathbf{x})}{\partial \boldsymbol{\nu}} + \frac{\partial \mathrm{Si}(\mathbf{x}_{jk}, \theta_{jk} \psi_q; \mathbf{x})}{\partial \boldsymbol{\nu}} \right) \mu_{jk,q}, \mathbf{x}_{jk} \in \Gamma_{jk}, \lambda_{jk,q} \in \mathbb{C}, \mu_{jk,q} \in \mathbb{C}, j, k = 1, \ldots, n_{el} \right\}. \tag{23}$$

Using these approximation spaces, the DEM elements Q^1-4-1, Q^1-8-2, Q^1-12-3, Q^1-16-4, and Q^1-20-5, where the superscript 1 refers to $\zeta = 1$, are constructed for the solution of the Helmholtz equation with a spatially variable wavenumber. These elements do not contain the contribution of the polynomial approximation Q_p for the reasons highlighted in Section 3. They are equipped with the following values of the angles ψ_q introduced in (23)

- Q^1-4-1: $\psi_1 = \pi/2$.
- Q^1-8-2: $\psi_1 = \arccos(0.5)$.
- Q^1-12-3: $\psi_1 = \arccos(0.707),\ \psi_2 = \pi/2$.
- Q^1-16-4: $\psi_1 = \arccos(0.75),\ \psi_2 = \arccos(0.2)$.
- Q^1-20-5: $\psi_1 = \arccos(0.9),\ \psi_2 = \arccos(0.5),\ \psi_3 = \pi/2$.

Note that the elements with an odd number of Lagrange multiplier degrees of freedom per edge, n_λ, use the last angle $\pi/2$ to generate only one Lagrange multiplier basis function (due to the ceiling/floor function in (23)) that is close to a constant function. Each of the other angles gives rise to two Lagrange multiplier basis functions.

4. Performance assessment

4.1. Model problem and computational setup

Here, the performance of the DEM elements proposed in the previous sections for the solution of Helmholtz problems with spatially varying wavenumbers is assessed. To this effect, the BVP (1) is considered for modeling the sound-hard scattering by a disk of radius 0.5 of a planar incident wave $e^{i\kappa \mathbf{d}^I \cdot \mathbf{x}}$, where $\mathbf{d}^I = [1, 0]$ is a unitary 2D vector representing the direction of incidence. The scatterer is assumed to be submerged in an acoustic fluid where the speed of sound varies in space. The computational domain Ω is chosen to be the two-dimensional domain delimited by the scatterer boundary $\partial\Omega_N$ (the circle of radius of 0.5 where the Neumann boundary condition is applied with $g_N = 0$), and the artificial boundary $\partial\Omega_R$ (the circle of radius 1.5 where the Robin boundary condition is applied with $g_R = i\kappa(\boldsymbol{\nu} \cdot \mathbf{d}^I - 1.0)e^{i\kappa \mathbf{d}^I \cdot \mathbf{x}}$ (see Fig. 4). Hence, the solution of the BVP (1) represents in this case the total pressure in the fluid medium. Two spatial distributions of the wavenumber are considered in the subsections below.

A sequence of increasingly refined uniform meshes are constructed for the chosen computational domain: they are characterized by n_r elements in the radial direction, and $n_\theta = 6n_r$ in the tangential direction. The number of elements in the radial direction, n_r, is varied between 8 and 80. Because an analytical solution of the chosen model problem is not available, a reference solution is computed instead using an even finer mesh with $n_r = 100$ and bi-pentic elements Q_5. Hence, this reference solution is computed using 1.5 million degrees of freedom.

In order to capture accurately the curved boundaries of the chosen computational domain, all considered polynomial elements Q_p are isoparametric, and the same geometrical mapping characterizing the isoparametric polynomial element of degree five is used for approximating these boundaries in all considered DEM elements.

The performance of each considered element is assessed by computing the relative error of the solution it delivers with respect to the reference solution. This relative error is evaluated on the set of nodes that are common to both the reference mesh and the computational mesh used for generating the numerical solution being assessed. If this solution is computed using DEM, its nodal values are defined by reconstructing at this node the DEM solutions associated with all elements attached to this node and averaging them. Hence, if $r(j)$ and $n(j)$, $j = 1, \ldots, n_m$ denote the indices of degrees of freedom of matching nodes of the reference mesh and mesh under consideration, respectively, the relative error is computed as

$$\textit{Relative error} = \sqrt{\frac{\sum_{j=1}^{n_m} \left(\mathbf{u}_{r(j)}^{ref} - \mathbf{u}_{n(j)}\right)^2}{\sum_{j=1}^{n_m} \mathbf{u}_{r(j)}^{ref\,2}}}.$$

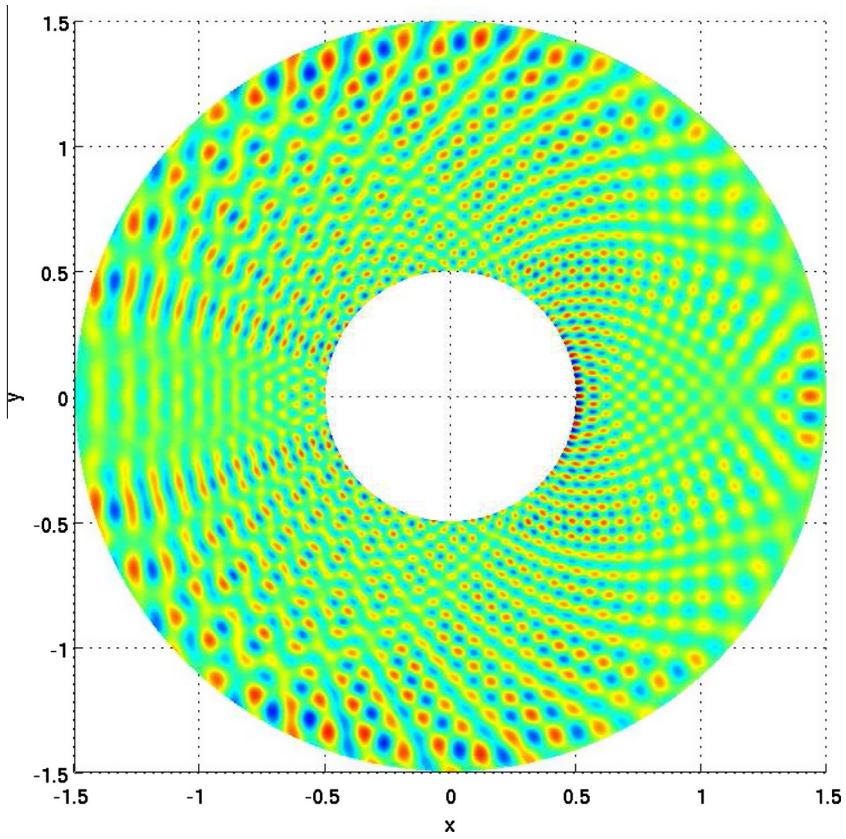

Fig. 4. Finite computational domain for a 2D scattering problem and contour plot of the real part of the numerical solution for the wavenumber $\kappa(\mathbf{x}(r)) = 160 - 80r$.

Static condensation is applied in both the considered DEM elements, whether these incorporate the discontinuous polynomial approximation or not, and the polynomial elements Q_p for which the degrees of freedom pertaining to interior nodes are eliminated. Table 1 summarizes the resulting degree of freedom counts for the considered elements and the mesh topology described above. These degree of freedom counts imply that the standard bi-polynomial element of degree p, Q_p, generates asymptotically slightly fewer degrees of freedom than a DEM element with $n_\lambda = p$ Lagrange multipliers per edge. However, the last column of Table 1 reveals that the matrices arising from a discretization by DEM are significantly sparser (see also [37]). For these reasons, and because for a constant wavenumber the elements Q_p and Q^0-4p-p were shown to exhibit the same convergence rate [7], each DEM element with $n_\lambda = p$ Lagrange multipliers is considered as a "comparable" to the standard element Q_p.

4.2. Radially variable wavenumber problem

The wavenumber is assumed to vary in space as

$$\kappa(\mathbf{x}(r)) = 160 - 80r, \tag{24}$$

where r is the distance from the center of the disk. This wavenumber: (1) is in the medium frequency regime, and (2) decreases in the radial direction from 120 next to the scatterer, to 40 on the artificial boundary. A numerical solution of the considered BVP with the variable wavenumber (24) is illustrated in Fig. 4.

Table 1
Computational complexity of the considered DEM and polynomial elements for a $n_r \times n_\theta$ uniform mesh.

Element type	Degree of freedom count	Maximum stencil width
Q_p	$(n_r+1)n_\theta + (2n_rn_\theta+1)(p-1) \approx n_rn_\theta(2p-1)$	$9+12(p-1)$
Q^0-n_w-n_λ	$(2n_rn_\theta-1)n_\lambda$	$7n_\lambda$
Q^0-n_w-p-n_λ	$(2n_rn_\theta-1)n_\lambda$	$7n_\lambda$
Q^1-n_w-n_λ	$(2n_rn_\theta-1)n_\lambda$	$7n_\lambda$

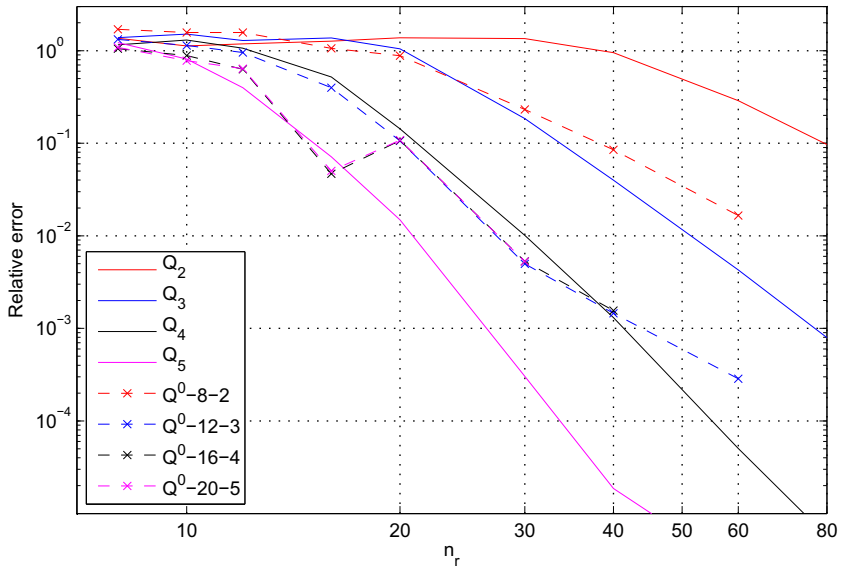

Fig. 5. Convergence comparison of the DEM elements Q^0-n_w-n_λ and the standard elements Q_p with $p = n_\lambda$ for $\kappa(\mathbf{x}(r)) = 160 - 80r$.

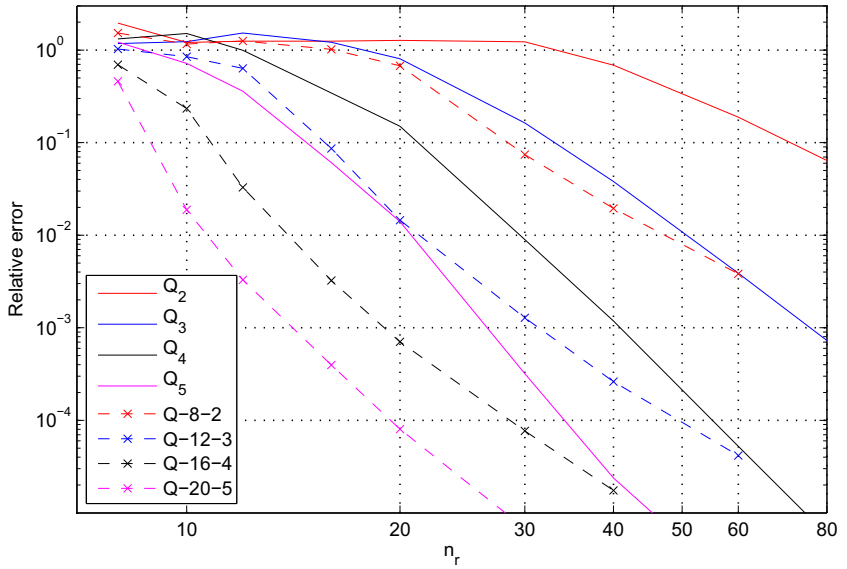

Fig. 6. Convergence comparison of the DEM elements Q-n_w-n_λ and the standard elements Q_p with $p = n_\lambda$ for $\kappa = 80$.

4.2.1. Performance assessment of the DEM elements Q^0-n_w-n_λ and Q^0-n_w-3-n_λ

First, each element Q^0-n_w-n_λ is benchmarked against its comparable standard polynomial finite element Q_p with $p = n_\lambda$. The lowest-order elements Q^0-4-1 and Q_1 are not considered as they are known to be computationally inefficient in the medium frequency regime. Fig. 5 shows that the DEM elements Q^0-n_w-n_λ deliver a respectable performance. For example, the DEM elements Q^0-8-2 and Q^0-12-3 outperform their comparable elements Q_2 and Q_3, respectively, as they achieve the same relative error using, in each case, a twice lower mesh resolution. However, Fig. 5 also reveals that the higher-order DEM elements Q^0-n_w-n_λ do not achieve for this problem a convergence improvement (cf. Section 3). Indeed, when the same BVP as above is considered but the wavenumber is fixed to the constant value $\kappa = 80$, Fig. 6 shows that all of the previously developed DEM elements Q-8-2, Q-12-3, Q-16-4, and the newly added element Q-20-5 outperform their polynomial counterparts Q_2, Q_3, Q_4, and Q_5, respectively. More specifically, these DEM elements deliver in this case the same accuracy as their standard polynomial counterparts using however a more than twice lower mesh resolution — that is, four times fewer degrees of freedom.

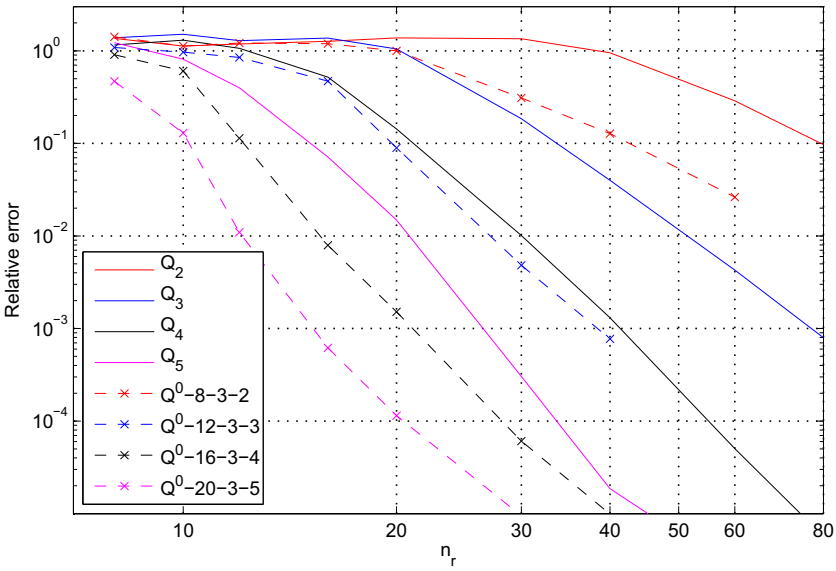

Fig. 7. Convergence comparison of the DEM elements Q^0-n_w-3-n_λ and the standard elements Q_p with $p = n_\lambda$ for $\kappa(\mathbf{x}(r)) = 160 - 80r$.

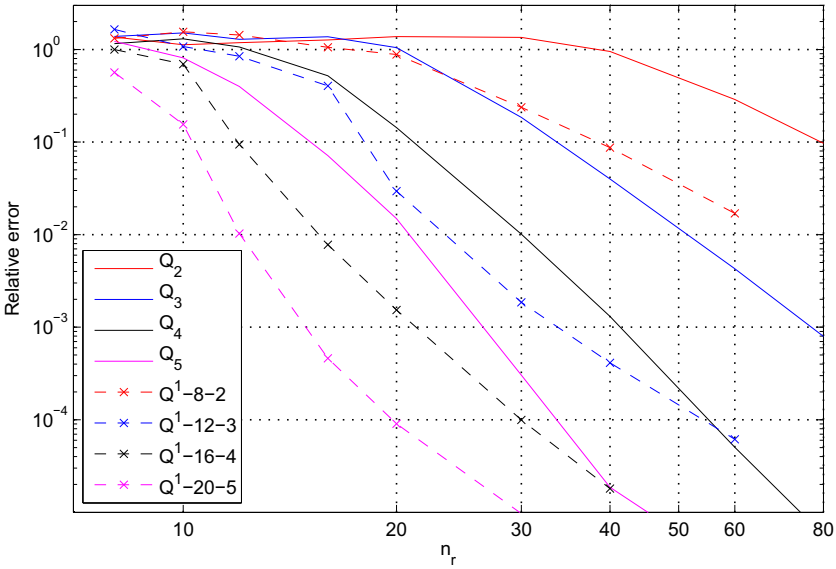

Fig. 8. Convergence comparison of the DEM elements Q^1-n_w-n_λ, the DEM elements Q^0-n_w-3-n_λ, and the standard elements Q_p with $p = n_\lambda$ for $\kappa(\mathbf{x}(r)) = 160 - 80r$.

Next, the performance of the DEM elements Q^0-n_w-3-n_λ is evaluated for the same BVP characterized by the variable wavenumber (24). The convergence results reported in Fig. 7 show that, as expected, adding the discontinuous bi-cubic polynomials to the approximation functions of the DEM elements Q^0-n_w-n_λ improves in this case significantly their performance at a modest increase of their computational complexity (thanks to the element-level static condensation). For example, the element Q^0-16-3-4 delivers the relative error of 10^{-4} using 27 elements in the radial direction, whereas its comparable bi-quartic continuous Galerkin element Q_4 requires more than 55 elements in this direction to achieve the same accuracy. This performance level of the DEM elements Q^0-n_w-3-n_λ for spatially variable wavenumbers is similar to the performance level of the DEM elements Q-n_w-n_λ for constant wavenumbers documented in the literature and Fig. 6.

4.2.2. Performance assessment of the DEM elements Q^1-n_w-n_λ

Finally, the performance of the DEM elements Q^1-n_w-n_λ based on the Airy plane waves is assessed against that of the standard polynomial finite elements Q_p with $p = n_\lambda$. It is noted that the Airy waves solve exactly a problem where the square of

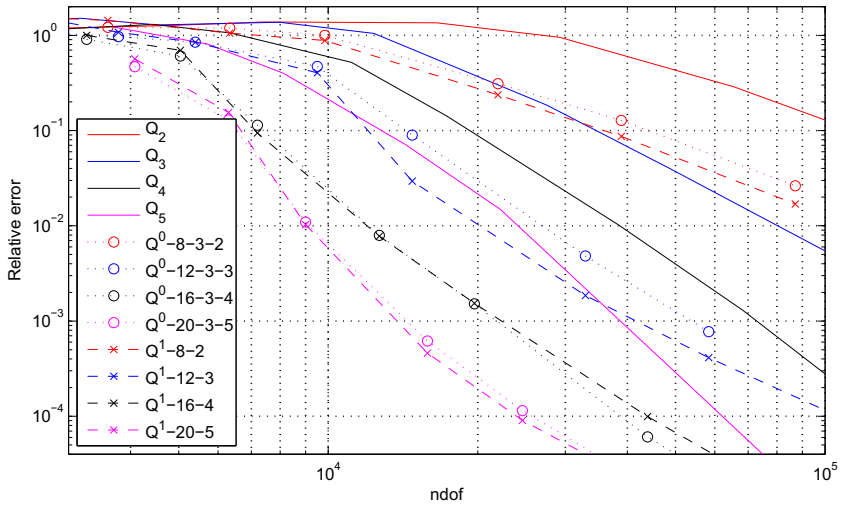

Fig. 9. Comparison of the relative errors achieved for a given degree of freedom count by the DEM elements Q^0-n_w-3-n_λ and Q^1-n_w-n_λ and the standard elements Q_p with $p = n_\lambda$ for $\kappa(\mathbf{x}(r)) = 160 - 80r$.

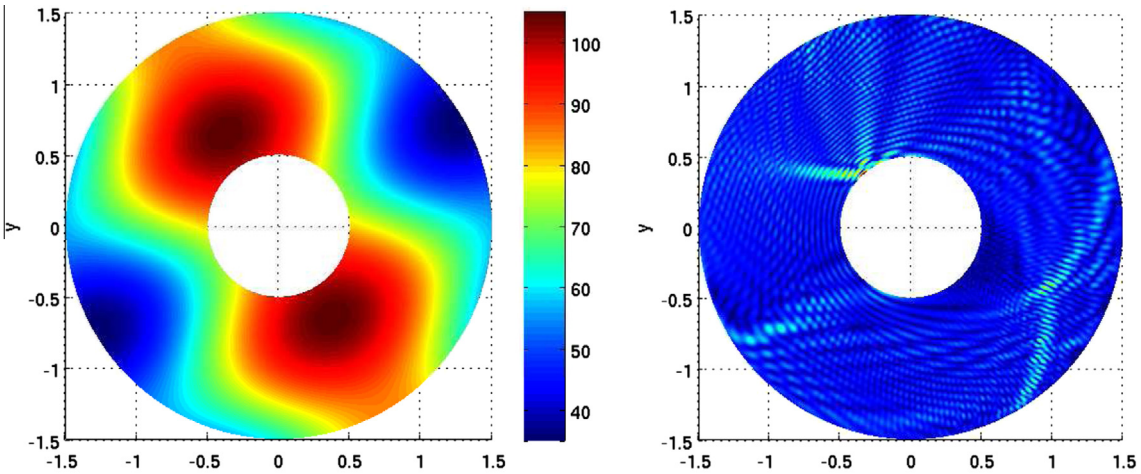

Fig. 10. The wavenumber distribution given by (25) (left); the pressure magnitude of the numerical solution (right).

the wavenumber is linear. However, for the problem at hand, the wavenumber itself varies linearly. Fig. 8 shows that each DEM element Q^1-n_w-n_λ outperforms its comparable polynomial finite element $Q_{p=n_\lambda}$ as it delivers the same accuracy but using a twice lower mesh resolution. A comparison with Fig. 7 also shows that each DEM element Q^1-n_w-n_λ delivers roughly the same performance as the DEM element Q^0-n_w-3-n_λ.

For completeness, the performance comparison of the DEM elements Q^1-n_w-n_λ, the DEM elements Q^0-n_w-3-n_λ, and the standard elements Q_p with $p = n_\lambda$ is illustrated in Fig. 9 in terms of degree of freedom count to achieve the same accuracy. The reader can observe that overall, the DEM elements Q^0-n_w-3-n_λ and Q^1-n_w-n_λ perform similarly, and each of them requires 3 to 5 times fewer degrees of freedom than their comparable standard polynomial element $Q_{p=n_\lambda}$ to deliver the same accuracy. Based on the two-dimensional comparative study performed in [37] for the case of a constant wavenumber, these savings can be reasonably expected to translate into more than one order of magnitude speedup of the global system solution time.

4.3. Asymmetrically variable wavenumber problem

The wavenumber is assumed to vary in space as

$$\kappa(x,y) = 75 + 25\cos\left(\frac{2\pi}{3}x'\right) + 10\cos\left(\frac{4\pi}{3}y' + \pi\right), \quad \begin{bmatrix} x' \\ y' \end{bmatrix} = \begin{bmatrix} \cos\frac{\pi}{6} & \sin\frac{\pi}{6} \\ -\sin\frac{\pi}{6} & \cos\frac{\pi}{6} \end{bmatrix} \begin{bmatrix} x \\ y \end{bmatrix} \tag{25}$$

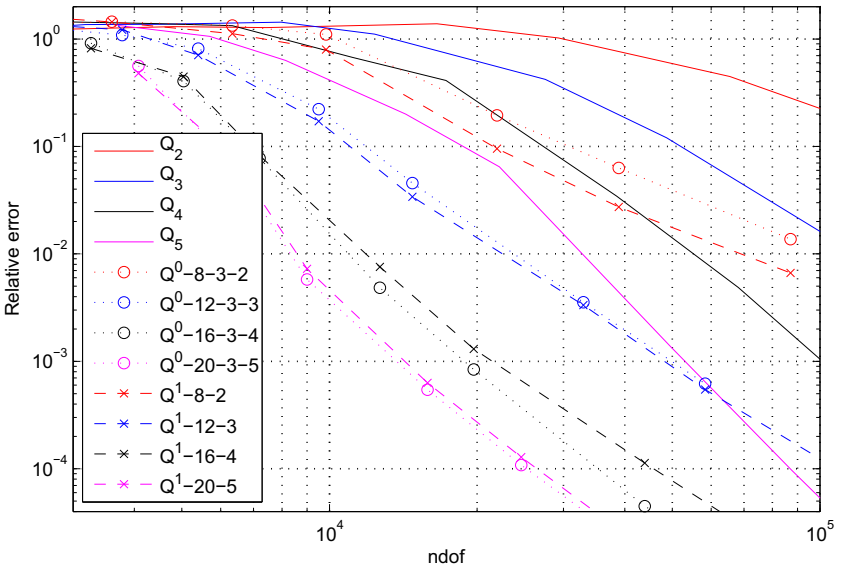

Fig. 11. Comparison of the relative errors achieved for a given degree of freedom count by the DEM elements Q^0-n_w-3-n_λ and Q^1-n_w-n_λ and the standard elements Q_p with $p = n_\lambda$ for the wavenumber given by (25).

This wavenumber varies from 40 to 110 and its distribution within the computational domain is depicted in Fig. 10 (left). The corresponding numerical solution of the considered BVP is shown in Fig. 10 (right).

The performance comparison of the DEM elements Q^1-n_w-n_λ, the DEM elements Q^0-n_w-3-n_λ, and the standard elements Q_p with $p = n_\lambda$ is illustrated in Fig. 11. For brevity, only the performance in terms of degrees of freedom is included here for this computational example. As in the previous computational example (cf. Fig. 9), the performance of the DEM elements Q^0-n_w-3-n_λ and Q^1-n_w-n_λ is similar, and 3 to 5 times fewer degrees of freedom deliver the accuracy of the comparable Galerkin polynomial element $Q_{p=n_\lambda}$.

5. Conclusions

In this paper, efficient DEM elements for the solution of time-harmonic wave propagation problems with a spatially variable wavenumber in the medium frequency regime have been constructed using free-space solutions of approximations of the underlying equation. The considered approximations of the Helmholtz equation in two dimensions have been obtained by successive Taylor series expansions of the wavenumber around a reference point. This has led to plane wave and Airy wave enrichment functions based on the piece-wise constant and linear approximations of the square of the wavenumber, respectively. Several two-dimensional elements based on these basis functions have been constructed. Their performance has been assessed and contrasted with that of the standard polynomial finite elements of comparable computational complexity for a benchmark problem modeling the sound-hard scattering by a disk of an incident wave in the medium frequency regime. It was found that the proposed DEM elements deliver the same accuracy as their counterpart polynomial elements using however three to five times fewer degrees of freedom, thereby validating the technical soundness of the proposed extension of the concept of free-space solutions. The ideas presented in this paper can be extended to three dimensions and this application will be presented in a future work.

Acknowledgment

Radek Tezaur and Charbel Farhat acknowledge the support by the Office of Naval Research under Grant N00014-05-1-0204-1.

References

[1] I. Babuška, J.M. Melenk, The partition of unity method, Int. J. Numer. Methods Engrg. 40 (1997) 727–758.
[2] O. Cessenat, B. Despres, Application of an ultra weak variational formulation of elliptic PDEs to the two-dimensional Helmholtz problem, SIAM J. Numer. Anal. 35 (1998) 255–299.
[3] R. Djellouli, C. Farhat, A. Macedo, R. Tezaur, Finite element solution of two-dimensional acoustic scattering problems using arbitrarily shaped convex artificial boundaries, J. Comput. Acoust. 8 (2000) 81–100.
[4] C. Farhat, I. Harari, L.P. Franca, The discontinuous enrichment method, Comput. Methods Appl. Mech. Engrg. 190 (2001) 6455–6479.
[5] C. Farhat, I. Harari, U. Hetmaniuk, The discontinuous enrichment method for multiscale analysis, Comput. Methods Appl. Mech. Engrg. 192 (2003) 3195–3210.

[6] C. Farhat, I. Harari, U. Hetmaniuk, A discontinuous Galerkin method with Lagrange multipliers for the solution of Helmholtz problems in the mid-frequency regime, Comput. Methods Appl. Mech. Engrg. 192 (2003) 1389–1419.
[7] C. Farhat, R. Tezaur, P. Wiedemann-Goiran, Higher-order extensions of a discontinuous Galerkin method for mid-frequency Helmholtz problems, Int. J. Numer. Methods Engrg. 61 (2004) 1938–1956.
[8] C. Farhat, P. Wiedemann-Goiran, R. Tezaur, A discontinuous Galerkin method with plane waves and Lagrange multipliers for the solution of short wave exterior Helmholtz problems on unstructured meshes, J. Wave Motion 39 (2004) 307–317.
[9] C. Farhat, I. Kalashnikova, R. Tezaur, A higher-order discontinuous enrichment method for the solution of high Péclet advection–diffusion problems on unstructured meshes, Int. J. Numer. Methods Engrg. 81 (2010) 604–636.
[10] G. Gabard, P. Gamallo, T. Huttunen, A comparison of wave-based discontinuous Galerkin, ultra-weak and least-square methods for wave problems, Int. J. Numer. Methods Engrg. 85 (2011) 380–402.
[11] E. Grosu, I. Harari, Studies of the discontinuous enrichment method for two-dimensional acoustics, Finite Elem. Anal. Des. 44 (2008) 272–287.
[12] E. Grosu, I. Harari, Three-dimensional element configurations for the discontinuous enrichment method for acoustics, Int. J. Numer. Methods Engrg. 78 (2009) 1261–1291.
[13] T. Huttunen, P. Monk, J.P. Kaipio, Computational aspects of the ultra-weak variational formulation, J. Comput. Phys. 182 (2002) 27–46.
[14] F. Ihlenburg, Finite Element Analysis of Acoustic Scattering, Springer-Verlag, New-York, 1998.
[15] L.-M. Imbert-Gerard, B. Després. Generalized plane wave numerical methods for magnetic plasma. in: Proceedings of the 10th International Conference on the Mathematical and Numerical Aspects of Waves Vancouver, Canada, 233–236, 2011.
[16] I. Kalashnikova, The Discontinuous Enrichment Method for Multi-Scale Transport Problems, Ph.D. Thesis, Stanford University, Stanford, CA, 2011.
[17] I. Kalashnikova, R. Tezaur, C. Farhat. A discontinuous enrichment method for variable coefficient advection–diffusion at high Péclet number, Int. J. Numer. Methods Engrg. 87 (2013) 309–335.
[18] Louis Kovalevsky, Pierre Ladevèze, Hervé Riou, The Fourier version of the variational theory of complex rays for medium-frequency acoustics, Comput. Methods Appl. Mech. Engrg. 225–228 (2012) 142–153.
[19] O. Laghrouche, P. Bettess, E. Perrery-Debain, J. Trevelyan, Plane wave basis finite-elements for wave scattering in three dimensions, Commun. Numer. Methods Engrg. 19 (2003) 715–723.
[20] O. Laghrouche, P. Bettess, E. Perrey-Debain, J. Trevelyan, Wave interpolation finite elements for Helmholtz problems with jumps in the wave speed, Comput. Methods Appl. Mech. Engrg. 194 (2005) 367–381.
[21] O. Laghrouche, A. El-Kacimi, J. Trevelyan, Extension of the PUFEM to elastic wave propagation in layered media, J. Comput. Acoust. 20 (2012) 2.
[22] T. Luostari, T. Huttunen, P. Monk, Improvements for the ultra weak variational formulation, Int. J. Numer. Methods Engrg. 94 (2013) 598–624.
[23] P. Massimi, R. Tezaur, C. Farhat, A Discontinuous enrichment method for three-dimensional multiscale harmonic wave propagation problems in multi-fluid and fluid–solid media, Int. J. Numer. Methods Engrg. 76 (2008) 400–425.
[24] P. Massimi, R. Tezaur, C. Farhat, A discontinuous enrichment method for the efficient solution of plate vibration problems in the medium-frequency regime, Int. J. Numer. Methods Engrg. 84 (2010) 127–148.
[25] J.M. Melenk, I. Babuška, The partition of unity method finite element method: basic theory and applications, Comput. Methods Appl. Mech. Engrg. 139 (1996) 289–314.
[26] P. Monk, D.Q. Wang, A least-squares method for the Helmholtz equation, Comput. Methods Appl. Mech. Engrg. 175 (1999) 121–136.
[27] P. Ortiz, E. Sanchez, An improved partition of unity finite element model for diffraction problems, Int. J. Numer. Methods Engrg. 50 (2001) 2727–2740.
[28] S. Petersen, C. Farhat, R. Tezaur, A space–time discontinuous Galerkin method for the solution of the wave equation in the time domain, Int. J. Numer. Methods Engrg. 78 (2008) 275–295.
[29] B. Pluymers, B. van Hal, D. Vandepitte, W. Desmet, Trefftz-based methods for time-harmonic acoustics, Arch. Comput. Methods Eng. 14 (2007) 343–381.
[30] A.D. Polyanin, V.F. Zaitsev, Handbook of Exact Solutions for Ordinary Differential Equations, 2nd Edition., Chapman & Hall, Boca Raton, FL, 2003.
[31] H. Riou, P. Ladevèze, B. Sourcis, The multiscale VTCR approach applied to acoustics problems, J. Comput. Acoust. 16 (4) (2008) 487–505.
[32] P. Rouch, P. Ladevèze, The variational theory of complex rays: a predictive tool for medium – frequency vibrations, Comput. Methods Appl. Mech. Engrg. 192 (2003) 3301–3315.
[33] T. Strouboulis, I. Babuška, R. Hidajat, The generalized finite element method for Helmholtz equation: theory, computation, and open problems, Comput. Methods Appl. Mech. Engrg. 195 (2006) 4711–4731.
[34] R. Tezaur, A. Macedo, C. Farhat, R. Djellouli, Three-dimensional finite element calculations in acoustic scattering using arbitrarily shaped convex artificial boundaries, Int. J. Numer. Methods Engrg. 53 (2002) 1461–1476.
[35] R. Tezaur, C. Farhat, Three-dimensional discontinuous Galerkin elements with plane waves and Lagrange multipliers for the solution of mid-frequency Helmholtz problems, Int. J. Numer. Methods Engrg. 66 (2006) 796–815.
[36] R. Tezaur, L. Zhang, C. Farhat, A discontinuous enrichment method for capturing evanescent waves in multiscale fluid and fluid/solid problems, Comput. Methods Appl. Mech. Engrg. 197 (2008) 1680–1698.
[37] D. Wang, R. Tezaur, J. Toivanen, C. Farhat, Overview of the discontinuous enrichment method, the ultra-weak variational formulation, and the partition of unity method for acoustic scattering in the medium frequency regime and performance comparisons, Int. J. Numer. Methods Engrg. 89 (4) (2012) 403–417.
[38] L. Zhang, R. Tezaur, C. Farhat, The discontinuous enrichment method for elastic wave propagation in the medium-frequency regime, Int. J. Numer. Methods Engrg. 66 (2006) 2086–2114.